Towards the characterization of the heat loss coefficient via on-board monitoring : physical interpretation of ARX model coefficients

Towards the Characterization of the Heat Loss Coefficient via On-Board Monitoring: Physical Interpretation of ARX Model Coefficients

Marieline Senave[1,2,3,*], Glenn Reynders[2,3], Peder Bacher[4], Staf Roels[1], Stijn Verbeke[2,3,5], Dirk Saelens[1,3]

[1]KU Leuven, Department of Civil Engineering, Building Physics Section, Belgium
[2]VITO, unit Smart Energy and Built Environment, Belgium
[3]EnergyVille, Cities in Transition, Belgium
[4]Technical University of Denmark, DTU Compute, Denmark
[5]University of Antwerp, Applied Engineering, EMIB, Belgium

[*]*Corresponding email: marieline.senave@kuleuven.be*

ABSTRACT
This paper explores the concept of characterizing the as-built Heat Loss Coefficient (HLC) of buildings based on on-board monitoring (OBM), via energy consumption and temperature sensors, and time series analysis. It is examined (1) how the coefficients of different Auto-Regressive with eXogenous inputs (ARX) models can be interpreted and (2) whether these conclusions are sensitive to the building envelope assembly or the applied indoor temperature profile.
The paper presents a theoretical case study whereby detailed building energy simulations are used to accurately map the impact of physical phenomena on the characterization process. The simulation models and boundary conditions are composed to focus on the link between the estimated ARX-coefficients and the physical driving forces for transmission heat loss to the ground and the exterior environment.
The results show how the various ARX model coefficients are linked to specific components of the HLC (e.g. heat transfer through the walls and roof or through the slab-on-ground floor) and to what extent they are affected by the selection of input variables. By monitoring the ground temperature, the transmission heat losses can rather accurately be assigned to either the slab-on-ground or the walls and roof. Without this measurement data, the uncertainty on the estimates increases (ranges of the 95% confidence interval of up to 35 % of the mean estimate). Modelling the ground heat losses by a constant intercept term leads to underestimations of the reference HLC of up to 59 %, whereas adding heat flux sensors to monitor the transmission heat losses to the ground to the measurement set-up allows to assess the transmission heat transfer coefficient to the exterior environment HLC_e within 2 %.

KEYWORDS
Characterization, Heat Loss Coefficient, ARX Modelling, Physical Parameter Identification, Synthetic Monitoring Data.

NOMENCLATURE

Variables	Symbol	Unit
Temperature	T	°C
Net heat input	Φ_h	W
Solar gains	Φ_{sol}	W
Internal heat gains	Φ_{int}	W
Heat transfer through transmission	Φ_{tr}	W
Heat transfer through infiltration	Φ_{inf}	W
Heat transfer through intended ventilation	Φ_v	W
Parameters		
Heat transfer coefficient by transmission	H_{tr}	W/K
Heat transfer coefficient by infiltration	H_{inf}	W/K
Heat loss coefficient	HLC	W/K

Thermal transmittance or U-value	U	W/m²K
Thermal resistance	R	m²K/W
Convective heat transfer coefficient	h_c	W/(m²K)
Radiative heat transfer coefficient	h_r	W/(m²K)
Surface area	A	m²

Subscripts	
Interior	i
Exterior	e
Ground	g
Sky	sky
Surface	s
Wall	W
Roof	R
Floor	F

1. INTRODUCTION

Knowledge of the as-built energy performance characteristics of buildings is important for on-site quality assessment and certification, the formulation of tailored retrofit strategies and financing plans for energy conservation measures, and the creation of reduced-order models for Model Predictive Control (MPC) and fault detection and diagnosis (FDD). One of the performance indicators of interest is the Heat Loss Coefficient (HLC), which describes the amount of heat input required to sustain a temperature difference of 1 K over the building envelope and is expressed in W/K.

HLC characterization techniques based on a combination of dedicated on-site tests and data-driven modeling, using linear regression [1,2], Auto-Regressive with eXogenous inputs ('ARX') models [3] or state-space models [4,5], show promising results regarding their accuracy. However, the applied steady-state heating experiments, such as the co-heating test [6,7], or the dynamic alternatives, such as the QUB test [8], ISABELE method [9] and Short Term Energy Monitoring (STEM) using PSTAR [10], involve costly measurement set-ups. They moreover require the building to be vacated for periods of a few days up to multiple weeks depending on the method. Given the rapid adoption of sensors in our everyday life and the European Commission's plea for the implementation and meaningful use of smart meters [11], it is analyzed whether on-board monitoring (OBM) can be used to capture the required data in a more practical way [12]. OBM is the monitoring of the energy use and indoor climate of in-use buildings, which are conditioned by the building's own HVAC devices, via non-intrusive sensing devices.

The presence of the occupants in the OBM set-up implies that the extent to which the building is excited is constrained by the thermal comfort requirements of the inhabitants. This altered experiment design calls for a thorough investigation of (1) the broader applicability of the data analysis techniques used on the data of the dedicated tests and (2) the physical meaning of the coefficients of the models identified from the data. For example, it needs to be verified whether the performance indicators inferred from on-board monitoring data equal the intrinsic characteristic of the building. Furthermore, the optimal sensor set-up of the OBM remains to be established under different circumstances (building typology, occupant behavior, etc.). Moreover, it is important to advance the understanding of the impact of missing input data on the accuracy of the characterization outcome.

This paper explores the potential for so-called 'in-use characterization' by performing case study analyses on synthetic data, from building models with clearly defined thermal performances, to examine whether and under which circumstances the outcome of an ARX-model applied on OBM-data can be related to the physical performance indicator 'HLC'. Focusing on identifying the transmission heat losses to the external environment and ground from the coefficients of the analysis model, the analyzed cases include different building assemblies and heating profiles. To support an in-depth analysis of the transmission heat loss, other physical phenomena occurring in in-use buildings, such as solar irradiation, internal gains and ventilation heat losses are disregarded.

The paper takes the Heat Loss Coefficient as a starting point and embeds it in a broader building

physical context (section 2). Next, the general principles of ARX-modelling are described. Section 4 links the previously derived heat balance equations to ARX-models under four different scenarios. This allows to formulate specific research questions and hypotheses. In the methodology section (section 5), the simulations executed to generate the case study data sets are detailed, as well as the applied ARX-models. The results are presented and analyzed in section 6. Finally, conclusions are drawn and future research questions are formulated.

2. BUILDING PHYSICAL BASIS: THE HEAT LOSS COEFFICIENT

The simplified steady-state heat balance of a single thermal zone (Eq. 1.1) states that the sum of the net heating power supplied by the heating system (Φ_h in W), the internal gains (Φ_{int}) and the solar gains through the transparent parts of the building envelope (Φ_{sol}) equals the heat transfer through transmission, infiltration and intended ventilation (Φ_{tr}, Φ_{inf} and Φ_v resp.). Ignoring the distinction between the equivalent temperature and air temperature [13], Φ_{tr} and Φ_{inf} can be written as respectively the heat transfer coefficient by transmission H_{tr} [W/K] and the heat transfer coefficient by infiltration H_{inf} [W/K] multiplied by the temperature difference between the interior and exterior environment (T_i and T_e are resp. the reference interior and exterior temperature in K) (Eq. 1.2). Although not unambiguously defined in an ISO-standard, a point that was also raised by [14], the Heat Loss Coefficient (HLC) is here referred to as the sum of H_{tr} and H_{inf} (Eq. 1.3), as is also done in [3,15].

$$\Phi_h + \Phi_{int} + \Phi_{sol} = -\Phi_{tr} - \Phi_{inf} - \Phi_v \quad (1.1)$$

$$= \left(H_{tr} + H_{inf}\right) \cdot (T_i - T_e) - \Phi_v \quad (1.2)$$

$$= HLC \cdot (T_i - T_e) - \Phi_v \quad (1.3)$$

Since this paper aims to prevail the way ARX-models capture transmission heat losses to the ambient and ground, the building model used in the case study simulations has been specifically constructed to support an in-depth analysis of these effects. The considered model represents a perfectly airtight, detached single-zone dwelling, constructed without thermal bridges. No ventilation system is foreseen, and solar and internal gains are set to zero. Hence in this case, Eq. 1 can be rewritten as Eq. 2 in which the net heat input compensates for the transmission heat losses to the exterior $\Phi_{tr,e}$ and ground $\Phi_{tr,g}$. The HLC thus only embeds the transmission heat transfer coefficient between the conditioned zone and the exterior ($H_{tr,e}$) and the transmission heat transfer coefficient through the ground ($H_{tr,g}$). These heat transfer coefficients can be expressed as demonstrated in Eq. 2.5 with A and U respectively the surface area [m²] and thermal transmittance [W/m²K] of the walls (subscript 'W') roof (subscript 'R') and floor (subscript 'F') separating the zone from the exterior environment and ground (ground temperature T_g).

$$\langle \Phi_{int} = \Phi_{sol} = \Phi_{inf} = \Phi_v = 0 \rangle \quad \& \quad \langle \Phi_{tr} = \Phi_{tr,e} + \Phi_{tr,g} \rangle \quad (2.1)$$

$$\Downarrow$$

$$\Phi_h = -\Phi_{tr,e} - \Phi_{tr,g} \quad (2.2)$$

$$= HLC \cdot (T_i - T_e) \quad (2.3)$$

$$= \left(H_{tr,e} + H_{tr,g}\right) \cdot (T_i - T_e) \quad (2.4)$$

$$= \left((A_w \cdot U_w + A_R \cdot U_R) + \left(A_F \cdot U_F \cdot \frac{(T_i - T_g)}{(T_i - T_e)}\right)\right) \cdot (T_i - T_e) \quad (2.5)$$

3. STATISTICAL BASIS: THE ARX-MODEL

Auto-Regressive models with eXogenous inputs (or abbreviated: 'ARX-models') can be used to identify and predict the behavior of linear and stationary (constant coefficients) dynamical systems, in this case: buildings [4]. The models, which can be classified as discrete time transfer function models, use linear difference equations to describe the relation between so-called 'input' and 'output' variables

(independent and depend variables resp.) [5,16]. By means of a backward shift operator B, past observations of the variables are factored in, as demonstrated in Eq. 3 with P_t the observation of variable P at time t.
A general example of an ARX-model that can be identified on monitoring data is shown in Eq. 4. It describes a multiple-input, single-output (MISO) system, with (the time series of) variable Y as output and X and Z as inputs. The polynomial $\varphi(B)$ of order n_φ in the backshift operator B holds the output or Auto-Regressive (AR) model coefficients as shown in Eq. 5. As can be seen, the order n determines the number of past observations that is taken into account. The input polynomials in B are denoted with ω. The polynomial of the variable X, $\omega_x(B)$, is defined in Eq. 6, $\omega_z(B)$ can be derived similarly. The estimated polynomials with the backshift operator B set equal to 1, for example $\omega_x(1)$, will further on be denoted as the 'steady-state gains' since they express the model's steady-state behavior. Finally, the term ε_t in Eq. 4 represents the one-step prediction error at time t.

$$B^k \cdot \boldsymbol{P_t} = \boldsymbol{P_{t-k}} \tag{3}$$

$$\varphi(B) \cdot \boldsymbol{Y_t} = \omega_x(B) \cdot \boldsymbol{X_t} + \omega_z(B) \cdot \boldsymbol{Z_t} + \varepsilon_t \tag{4}$$

$$\varphi(B) = 1 + \varphi_1 \cdot B^1 + \varphi_2 \cdot B^2 + \cdots + \varphi_{n_\varphi} \cdot B^{n_\varphi} \tag{5}$$

$$\omega_x(B) = \omega_{x,0} + \omega_{x,1} \cdot B^1 + \cdots + \omega_{x,n_x} \cdot B^{n_x} \tag{6}$$

4. LINKING THE BUILDING PHYSICAL AND STATISTICAL FRAMEWORK UNDER 4 SCENARIOS

In what follows, the heat balance without accounting for solar and internal gains or ventilation losses (Eq. 2) will be further developed and linked to specific ARX-parametrizations. ARX-models are generally classified as 'black-box models', which in principle have no prior physical knowledge incorporated into their model structure. The models merely rely on the statistical correlations present in the measurement data to express the output variable in function of the input data. Therefore, the identified model coefficients do not necessarily relate to physical parameters. Moreover, the ARX models describe the buildings' dynamic behavior, whereas the HLC as defined in section 2 is a steady-state performance indicator.
Since in this study the ARX models are identified on actual physical variables such as temperatures and heat flow rates, it is assumed here that the model coefficients of ARX models fitted to OBM data do have a physical meaning. By linking the equations of the building physical and statistical basis, an attempt is made to deduce this meaning and unriddle the issue concerning the steady-state versus dynamic behavior.
Four scenarios, differing in either the experimental design of the OBM or the assumptions made during data analysis, are considered:

- Scenario 1 (s1) assumes the ideal situation in which the ground temperature T_g is monitored and modelled explicitly.
- Since monitoring data of T_g is typically not available for actual in-use buildings, Scenario 2 (s2) considers disregarding the ground heat losses.
- Scenario 3 (s3) explores the added value of measuring the heat flux through the slab-on-ground on the identifiability of the HLC.
- Finally, in a fourth scenario (s4) it is examined whether using a synthetic deep ground temperature ('T_{g_deep}') during data analysis can function as an alternative for monitoring T_g.

4.1. Scenario 1: Ground temperature (T_g) is monitored

In this first scenario, we assume that the net heat input and all temperatures (the interior and exterior as well as the ground temperature) are monitored. Rewriting Eq. 2.5 in terms of these variables yields the following expression (Eq. 7):

$$\Phi_h = (A_w \cdot U_w + A_R \cdot U_R + A_F \cdot U_F) \cdot T_i - (A_w \cdot U_w + A_R \cdot U_R) \cdot T_e - (A_F \cdot U_F) \cdot T_g \tag{7}$$

In the above equation three different constituents or variants of the HLC can be discerned. The coefficient of T_i describes the overall transmission heat loss through the entire envelope and will from now on be referred to as 'HLC_i'. The coefficient of T_e represents a second performance indicator, 'HLC_e', which expresses the transmission heat loss per degree Kelvin temperature difference over the building elements in contact with the exterior environment (the walls and roof). Finally, the product of the surface area and thermal transmittance of the slab-on-ground will be denoted as 'HLC_g'. Notably, HLC_i [W/K] is the sum of HLC_e and HLC_g.
All HLC-definitions are summarized in Table 1, and they were used to translate Eq. 7 into Eq. 8A. Eq. 8A can furthermore be rewritten with T_i as dependent variable, which results in variant Eq. 8B.

$$\Phi_h = HLC_i \cdot T_i - HLC_e \cdot T_e - HLC_g \cdot T_g \quad (8A)$$

$$HLC_i \cdot T_i = \Phi_H + HLC_e \cdot T_e + HLC_g \cdot T_g \quad (8B)$$

Table 1.

Parameter:	Physical formula
HLC:	$(A_w \cdot U_w + A_R \cdot U_R) + \left(A_F \cdot U_F \cdot \frac{(T_i - T_g)}{(T_i - T_e)}\right)$
HLC_i:	$A_w \cdot U_w + A_R \cdot U_R + A_F \cdot U_F$
HLC_e:	$A_w \cdot U_w + A_R \cdot U_R$
HLC_g:	$A_F \cdot U_F$

Based on these physical equations (Eqs. 8) the two ARX-parametrizations shown in Eqs. 9 can be drawn up. The first one, Eq. 9A, is a MISO-model with the time series of the net heat input as output and the three temperature variables as inputs. Similar to Eq. 8B, the model described in Eq. 9B uses a set-up with the interior temperature as output.

$$\varphi(B) \cdot \boldsymbol{\Phi_{h;t}} = \omega_i(B) \cdot \boldsymbol{T_{i;t}} + \omega_e(B) \cdot \boldsymbol{T_{e;t}} + \omega_g(B) \cdot \boldsymbol{T_{g;t}} + \varepsilon_t \quad (9A)$$

$$\varphi(B) \cdot \boldsymbol{T_{i;t}} = \omega_h(B) \cdot \boldsymbol{\Phi_{h;t}} + \omega_e(B) \cdot \boldsymbol{T_{e;t}} + \omega_g(B) \cdot \boldsymbol{T_{g;t}} + \varepsilon_t \quad (9B)^1$$

To analyze the monitoring data of controlled co-heating tests with constant indoor temperature, linear regression or ARX-models with ϕ_h as output, such as Eq. 9A, are generally preferred [3,4]. For the data collected during dynamic tests, on the other hand, preference is generally given to variant 9B. Here, the interior temperature is assumed to depend on the imposed heating signal (e.g. a Pseudorandom Binary Sequence (PRBS)) [4,17]. In the context of in-use buildings, neither a constant temperature profile during day and night nor pronounced discontinuities in the heat input are likely, hence, both approaches (Eq. 9A or 9B) will be tested. Nevertheless, extra care needs to be taken when interpreting the results of the models with ϕ_h as output, since [18] points out that for this type of transfer function models causality issues might arise due to the non-negligible thermal capacity of the interior air.

Given the close resemblance between Eqs. 8 and 9, this research will investigate whether the steady-state gains from the output and input variables correspond to the three HLC's as postulated in Eqs. 10A (for model set-ups with Φ_h as output) and 10B (for model set-ups with T_i as output).

$$\frac{\omega_i(1)}{\varphi(1)} \stackrel{?}{=} HLC_i \qquad \frac{\omega_e(1)}{\varphi(1)} \stackrel{?}{=} HLC_e \qquad \frac{\omega_g(1)}{\varphi(1)} \stackrel{?}{=} HLC_g \quad (10A)$$

$$\frac{\varphi(1)}{\omega_h(1)} \stackrel{?}{=} HLC_i \qquad \frac{\omega_e(1)}{\omega_h(1)} \stackrel{?}{=} HLC_e \qquad \frac{\omega_g(1)}{\omega_h(1)} \stackrel{?}{=} HLC_g \quad (10B)$$

[1]The values of the output and input polynomials ϕ and ω in Eqs. 9A and B are not necessarily equal.

4.2. Scenario 2: No data on ground heat losses available

In the second, more practical scenario, the ground temperature is not monitored. Eq. 11A shows how Φ_h can be expressed in function of the two remaining temperatures T_i and T_e. The ground temperature T_g is implicitly accounted for by a temperature correction factor embedded in the HLC (see Table 1).

$$\Phi_h = HLC \cdot T_i - HLC \cdot T_e \quad (11A)$$

$$HLC \cdot T_i = \Phi_h + HLC \cdot T_e \quad (11B)$$

This steady-state heat balance can be approximated by the ARX-models in Eqs. 12A and B.

$$\varphi(B) \cdot \boldsymbol{\Phi_{h;t}} = \omega_i(B) \cdot \boldsymbol{T_{i;t}} + \omega_e(B) \cdot \boldsymbol{T_{e;t}} + \varepsilon_t \quad (12A)$$

$$\varphi(B) \cdot \boldsymbol{T_{i;t}} = \omega_h(B) \cdot \boldsymbol{\Phi_{h;t}} + \omega_e(B) \cdot \boldsymbol{T_{e;t}} + \varepsilon_t \quad (12B)$$

In Eqs. 11 the coefficients of both T_i and T_e equal the HLC. It is therefore hypothesized that the ratio of the steady-state gains of T_i and Φ_h (which will further be denoted as 'H_i') corresponds to the ratio of the steady-state gains of T_e and Φ_h (which will further be denoted as 'H_e'). Using Lagrange weighting, a method suggested by [4,19], H_i and H_e will then be combined into one single HLC estimate. As expressed in Eq. 14, a Lagrange multiplier λ is determined, which considers both the variance ('Var') and covariance ('Cov') of H_i and H_e. By using λ as a weighting factor in Eqs. 13, the parameter of the two with the lowest variance receives the highest weight and vice versa.

$$\left(\frac{\omega_i(1)}{\varphi(1)} = H_i\right) \stackrel{?}{=} \left(H_e = \frac{\omega_e(1)}{\varphi(1)}\right) \quad \rightarrow \quad \lambda \cdot H_i + (1-\lambda) \cdot H_e = H \stackrel{?}{=} HLC \quad (13A)$$

$$\left(\frac{\varphi(1)}{\omega_h(1)} = H_i\right) \stackrel{?}{=} \left(H_e = \frac{\omega_e(1)}{\omega_h(1)}\right) \quad \rightarrow \quad \lambda \cdot H_i + (1-\lambda) \cdot H_e = H \stackrel{?}{=} HLC \quad (13B)$$

$$\lambda = \frac{Var(H_e) - Cov(H_i, H_e)}{Var(H_i) + Var(H_e) - 2 \cdot Cov(H_i, H_e)} \quad (14)$$

In his research on HLC characterization via in-situ co-heating tests [3] examined the way ARX model coefficients can be interpreted as well. He uses the ARX-model described in Eq. 12A, with an extra input term added to explicitly include the incident solar radiation. For a case-study such as the ones studied here (a detached dwelling without cellar), Bauwens however suggests using $\omega_i(1)/\varphi(1)$ to assess the HLC_i. He furthermore states that $\omega_e(1)/\varphi(1)$ results in an HLC excluding the heat loss to the ground, here denoted as HLC_e.
The research will thus have to point out whether his [3] guidelines can be extended to the considered OBM-cases investigated under scenario 2, or Eqs. 13A and B provide a better approach.

4.3. Scenario 3: Transmission heat losses to the ground ($\Phi_{tr,g}$) are monitored

In Scenario 3, the monitoring set-up is extended with heat flux sensors mounted on the indoor surface of the slab-on-ground. Under the crude assumption that these local measurements are representative for the entire transmission heat loss to the ground, $\Phi_{tr,g}$ can hence be approximated as the monitored heat flux times the surface area of the floor slab. Summing this variable and the net heat input Φ_h yields the sum of the U-values multiplied by the surface areas of the walls and roof, denoted as HLC_e, as the coefficient of T_i and T_e (Eqs. 15 and 16).

$$\Phi_h + \Phi_{tr,g} = -\Phi_{tr,e} \quad (15.1)$$

$$= (A_w \cdot U_w + A_R \cdot U_R) \cdot T_i - (A_w \cdot U_w + A_R \cdot U_R) \cdot T_e \quad (15.2)$$

$$\Phi_h + \Phi_{tr,g} = HLC_e \cdot T_i - HLC_e \cdot T_e \quad (16A)$$

$$HLC_e \cdot T_i = \left(\Phi_h + \Phi_{tr,g}\right) + HLC_e \cdot T_e \quad (16B)$$

The ARX models corresponding to the heat balance Eqs. 16 are listed in Eqs. 17, with the sum of Φ_h and $\Phi_{tr,g}$ as a combined output or input in set-up A and B resp.

$$\varphi(B) \cdot \left(\boldsymbol{\Phi_{h;t}} + \boldsymbol{\Phi_{tr,g;t}}\right) = \omega_i(B) \cdot \boldsymbol{T_{i;t}} + \omega_e(B) \cdot \boldsymbol{T_{e;t}} + \varepsilon_t \quad (17A)$$

$$\varphi(B) \cdot \boldsymbol{T_{i;t}} = \omega_h(B) \cdot \left(\boldsymbol{\Phi_{h;t}} + \boldsymbol{\Phi_{tr,g;t}}\right) + \omega_e(B) \cdot \boldsymbol{T_{e;t}} + \varepsilon_t \quad (17B)$$

Similar to scenario 2, two parameters H_i and H_e will be derived from the steady-state gains and subjected to a minimum variance weighting, this time to approximate HLC_e.

$$\left(\frac{\omega_i(1)}{\varphi(1)} = H_i\right) \stackrel{?}{=} \left(H_e = \frac{\omega_e(1)}{\varphi(1)}\right) \quad \rightarrow \quad \lambda \cdot H_i + (1-\lambda) \cdot H_e = H \stackrel{?}{=} HLC_e \quad (18A)$$

$$\left(\frac{\varphi(1)}{\omega_h(1)} = H_i\right) \stackrel{?}{=} \left(H_e = \frac{\omega_e(1)}{\omega_h(1)}\right) \quad \rightarrow \quad \lambda \cdot H_i + (1-\lambda) \cdot H_e = H \stackrel{?}{=} HLC_e \quad (18B)$$

4.4. Scenario 4: Data analysis using a synthetic deep ground temperature (T_{g_deep})

In this final scenario, we aim to compensate for a lack of measurement data of T_g by using a synthetically generated time series of the (undisturbed) deep ground temperature, T_{g_deep}, during data analysis. Hence, Eqs.7-9 from scenario 1 apply here as well, with T_g substituted by 'T_{g_deep}'. The steady-state gains will also be handled in a similar way in order to extract an estimate for HLC_i, HLC_e and HLC_g. Since the ground temperature profile T_{g_deep} is extracted at greater depth compared to T_g, the implicitly embedded resistance of the soil may yield lower estimates for HLC_i and HLC_g than the calculated reference values (Eqs. 19).

$$\frac{\omega_i(1)}{\varphi(1)} \stackrel{?}{<} HLC_i \qquad \frac{\omega_e(1)}{\varphi(1)} \stackrel{?}{=} HLC_e \qquad \frac{\omega_g(1)}{\varphi(1)} \stackrel{?}{<} HLC_g \quad (19A)$$

$$\frac{\varphi(1)}{\omega_h(1)} \stackrel{?}{<} HLC_i \qquad \frac{\omega_e(1)}{\omega_h(1)} \stackrel{?}{=} HLC_e \qquad \frac{\omega_g(1)}{\omega_h(1)} \stackrel{?}{<} HLC_g \quad (19B)$$

5. RESEARCH METHODOLOGY: CASE STUDIES

To accurately know the reference HLC's and to ensure that divers scenarios can be easily considered, the characterization exercise is conducted on synthetic data sets, generated with the Building Energy Simulation software TRNSYS 17 [20]. Although a formal validation is not possible in this study, TRNSYS has been extensively tested with good results against both analytical standards [21,22] and experimental data [23]. The case study simulations are described in section 5.1, after which section 5.2 details the reference HLC values. More information on the data analysis with ARX-models is provided in section 5.3.

5.1. Building Energy Simulations

As case study object, a single-zone opaque box of 7m*5m*3m (length*width*height), is modelled with TRNSYS type 56 [24]. To analyze the characterization process' sensitivity to (1) the thermal transmittance of the roof, walls and floor and (2) the interior temperature, four different levels of thermal resistance of the building envelope and four distinct set point temperature profiles for space heating are considered as explained below.

As discussed in section 4, a distinction can be made between the thermal performance of the building elements in contact with the exterior (roof and walls) and the slab-on-ground (performance indicators 'HLC_e' and 'HLC_g', resp.). Therefore, this study will consider four options for the envelope composition, with either thermal insulation solely in roof and walls, solely in the floor slab, in all constructions or no thermal insulation at all. Table 2 details the four sets of assemblies that were defined. The variants will henceforth be denoted by two capital letters with subscripts. The letters describe a level of thermal resistance: either low ('L') or high ('H'). The first letter concerns the thermal resistance of the building

elements in contact with the exterior environment, as indicated by the subscript 'E'. The second letter points to the thermal resistance of the slab-on-ground (subscript 'G' for 'Ground'). Hence, 'L_EH_G' for example refers to the TRNSYS model with a relatively low thermal resistance between the interior and exterior environment but a highly insulated floor slab.

Table 2: Overview of the material layers present in the roof, walls and floor of the four defined cases, as well as the overall thermal resistance of the material layers R_{ML} (Eq.20).

			Material Layers Present				R_{ML} [m²K/W]			
		Case	L_EL_G	L_EH_G	H_EL_G	H_EH_G	L_EL_G	L_EH_G	H_EL_G	H_EH_G
Exterior environment	Roof	reinforced concrete slab	✓	✓	✓	✓	0.223	0.223	5.94	5.94
		screed to falls	✓	✓	✓	✓				
		thermal insulation (PUR)			✓	✓				
		weatherproof membrane	✓	✓	✓	✓				
	Walls	inner leaf	✓	✓	✓	✓	0.327	0.327	6.12	6.12
		air cavity	✓	✓						
		thermal insulation (mineral wool)			✓	✓				
		outer leaf	✓	✓	✓	✓				
Ground	Floor	screed	✓	✓	✓	✓	0.179	5.89	0.179	5.89
		thermal insulation (PUR)		✓		✓				
		reinforced concrete slab	✓	✓	✓	✓				

Space heating is provided by a simplified, 100 % convective heating system, the power of which is limited to the power needed to meet the heat demand on the coldest day[2]; 5.7, 1.8, 5.3 and 1.2 kW respectively for cases L_EL_G, H_EL_G, L_EH_G and H_EH_G.

Since the aim is to mimic data collected during OBM, the system is simulated to operate according to heating strategies commonly applied in occupied dwellings. In total, four set point temperature profiles have been specified, differing in amount of variance imposed on the interior air temperature. As can be seen in Figure 1, profile 1 ('P1') is characterized by a limited night set-back from 10 PM to 7 AM. Profile 2 ('P2') represents a situation in which the building is heated during morning and evening on working days. During the weekend the heating system is active during the entire day. The set-back is considerably lower than the temperature during occupation. The third profile ('P3') follows the same schedule during the entire week The set-back is less pronounced than the set-back applied on weekdays for profile 2. Finally, a constant setpoint temperature profile was added, similar to the one used during co- heating tests (labelled 'CH').
Throughout the paper the different simulations will be referred to using a combination of the label describing the assembly of the building envelope and the label denoting the applied set point temperature profile, such as for example: 'L_EH_G_P3' or 'H_EH_G_CH'.

[2] Climate data is discussed further on

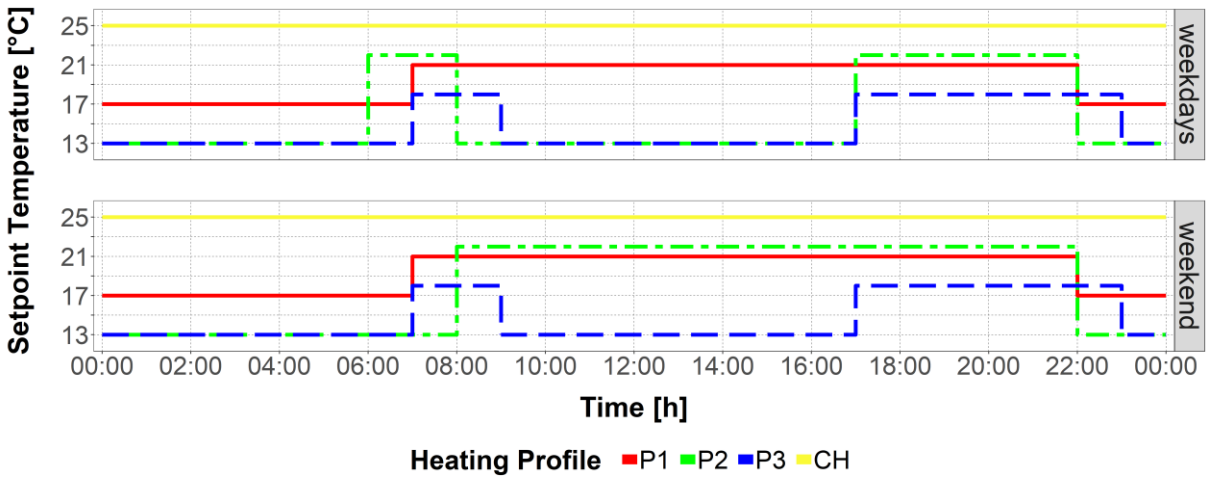

Figure 1: The setpoint temperature profiles for the heating of the zone air that will be explored throughout the different case studies.

In each of the sixteen scenarios the TMY2 climate dataset of Brussels (Belgium) was applied to represent typically encountered weather conditions. The building to ground energy exchange was modelled via TRNSYS Type 49 [25], assuming the following properties for the soil mass: thermal conductivity of 2 W/mK and density of 2000 kg/m³, average surface soil temperature 10 °C, amplitude of soil surface temperature: 7 °C and 'day of minimum surface temperature': 33 (ISO 13370, 2017a; Schietecat, 2002).
Furthermore, a temperature profile for undisturbed soil at 7 m depth was generated by TRNSYS Type 501.
Neither solar irradiation nor internal gains are modelled. The zone air is furthermore assumed to be perfectly mixed and no air exchanges by ventilation or infiltration through the envelope are considered.

The simulation output is generated with a sampling time of 3 minutes. This original output data is later on resampled to hourly values.

5.2. Determination of Reference HLC Value

For each of the case study simulations the reference HLC, HLC_i, HLC_e and HLC_g values are determined to enable the verification of the ARX characterization outcomes. Since these performance indicators are not directly available as simulation output, they are obtained using the procedure described below.

The HLCs of the box buildings can be calculated as the product of the surface areas and thermal transmittances of the building elements (Eqs. 2.3-5). Eq. 20 illustrates how the thermal transmittance of a thermally homogeneous building element x equals the inverse of its total thermal resistance R_{tot} [m²K/W], which in turn is the sum of the thermal resistances of the internal and external surface (R_{si} and R_{se} resp.) and the thermal resistances of the *n* material layers $R_1, R_2 \dots R_n$ in the element. These latter ones can be calculated as the quotients of the layer thicknesses and thermal conductivities and the R_{ML}-values are listed in Table 2.

$$U_x = \frac{1}{R_{tot,x}} = \frac{1}{(R_{si,x}+R_{ML,x}+R_{se,x})} = \frac{1}{(R_{si,x}+(R_{1,x}+R_{2,x}+\cdots+R_{n,x})+R_{se,x})} \quad (20)$$

Instead of adding the standard values of surface thermal resistances R_{se} and R_{si} specified in (ISO 6946, 2017) to determine R_{TOT}, the arithmetic mean is taken of the actual hourly values of these parameters, which can be manually calculated from the TRNSYS outputs using Eqs. 21-23. Hence, this implies that the reference values with which the results will be compared are not the 'theoretical' values as determined by the governing standards, but the actual values as used by TRNSYS.
$T_{si,x}$ in Eq. 21 stands for the interior surface temperature of building elements x, T_{STAR} for the star

temperature of the interior zone (see further, 5.3.1) and $\phi_{comi,x}$ for the heat flow rate from the inside surface of building elements x[3].
h_{ce} and h_{re} in Eq. 22 respectively represent the convective and radiative heat transfer coefficient of the external surface [W/(m²K)]. σ in Eq. 23 is the Stefan-Boltzmann constant [W/(m²K⁴)] and e_L the hemispherical emissivity of the surface (here taken equal to 0.9). T_{sky} is the sky temperature and $T_{se,x}$ the exterior surface temperature of building elements x[4]. Finally, v_{ssky} represents the view factor from the building elements' external surface to the sky. For the walls, roof and floor v_{ssky} is respectively set equal to 0.5, 1 and 0. To calculate h_{re} the ground surface temperature is assumed to equal the exterior air temperature.

$$R_{si,x} = \frac{A_x \cdot (T_{si,x} - T_{STAR})}{Q_{comi,x}} \quad (21)$$

$$R_{se,x} = \frac{1}{(h_{ce,x} + h_{re,x})} \quad (22)$$

$$h_{re,x} = \sigma \cdot e_L \cdot \frac{\left(T_{se,x}{}^4 - \left(v_{ssky,x} \cdot T_{sky} + (1 - v_{ssky},x) \cdot T_{air,e}\right)^4\right)}{\left(T_{se,x} - \left(v_{ssky,x} \cdot T_{sky} + (1 - v_{ssky},x) \cdot T_{air,e}\right)\right)} \quad (23)$$

The resulting HLC values are summarized in Table 3. Since the temperature correction factor $(T_i - T_g)/(T_i - T_e)$ is on average lower than 1 for all cases, the HLC values are lower than the HLC_i's. The latter yield the sum of the HLC_e's and HLC_g's. The HLC_e values of cases L_EL_G and L_EH_G, as well as H_EL_G and H_EH_G are, evidently, equal given their identical wall and roof assemblies. The same holds for the HLC_g values of cases L_EL_G and H_EL_G as well as L_EH_G and H_EH_G.

Table 3: Reference values of the HLCs. The values are presented per insulation level of the building envelope and indicate the 'mean (+-standard deviation)' of the reference values for the four imposed heating profiles P1, P2, P3 and CH.

	Cases			
	L_EL_G	**L_EH_G**	**H_EL_G**	**H_EH_G**
HLC [W/K]	282 (+-2.69)	264 (+-0.58)	42.7 (+-1.41)	21.0 (+-0.22)
HLC_i [W/K]	367 (+-0.76)	267 (+-0.01)	124 (+-0.00)	23.1 (+-0.00)
HLC_e [W/K]	261 (+-0.35)	261 (+-0.01)	17.3 (+-0.00)	17.3 (+-0.00)
HLC_g [W/K]	106 (+-0.41)	5.79 (+-0.00)	107 (+-0.00)	5.79 (+-0.00)
HLC_e/ HLC_i [%]	71.0 (+-0.05)	97.8 (+-0.00)	13.9 (+-0.00)	74.9 (+-0.00)

5.3. Data Analysis Using ARX-Models

Data analysis is carried out using R [29]. The following subsections will successively discuss the input data and model parametrizations used (5.3.1); the adopted model order selection procedure (5.3.2); the applied validation tests (5.3.3) and the identification of the HLC (5.3.4).

5.3.1. Input data and model parametrization

The variables used as output ['o'] or input ['i'] of the ARX-models are:

- **$\underline{T_i}$** ['o' or 'i']**:** The interior equivalent temperature [°C], here represented by TRNSYS Type 56 variable T_{STAR}, which is a direct simulation output calculated per zone.
  TRNSYS' standard radiation model approximates the interior zone by a star network. The artificial

[3] ϕ_{comi} [W] is the "combined energy from the inside surface including convection to air and longwave radiation to other surfaces" [24]

[4] Both the surface temperatures of the building elements and the heat flow rates through them are assumed to be uniform.

temperature node T_{STAR}, central to this network, considers both the longwave radiation exchange between the interior surfaces within the zone and the energy flow by convection between the interior surfaces and the zone air node [24].
It is important to emphasize that the interior equivalent temperature is related to the interior surface temperatures and thus is different than the thermostatically controlled interior mean air temperature (the setpoint temperatures shown in Figure 1).

- **$\underline{T_e}$** ['i']**:** The (overall) exterior equivalent temperature [°C]. This time series is determined as a surface area weighted average of the individual exterior equivalent temperatures of the four walls and roof. The exterior equivalent temperature of a building element x, $T_{equiv,e,x}$, is hereby obtained by applying Eq. 24.

$$T_{equiv,e,x} = \frac{\Phi_{como,x} \cdot R_{se,x}}{A_x} + T_{se,x} \tag{24}$$

with $\phi_{como,x}$ the heat flow rate to the outside surface of building element x ("including convection to air and longwave radiation to other surfaces or T_{sky}", [24]), and $T_{se,x}$ the exterior surface temperature of the building element. Both variables are direct simulation outputs.

- **$\underline{T_g}$** ['i']**:** The ground temperature [°C], which is calculated as $T_{equiv,e,floor}$ (Eq. 24).
- **$\underline{T_{g\ deep}}$** ['i']**:** The undisturbed ground temperature at 7 m depth [°C], a direct simulation output.
- **$\underline{\Phi_h}$** ['o' or 'i']**:** The net heat input in W, a direct simulation output.
- **$\underline{\Phi_{tr,g}}$** ['o' or 'i']**:** The transmission heat flow through the floor slab to the ground [W], calculated as Eq. 25.

$$\Phi_{tr,g} = \frac{A_F \cdot (T_g - T_i)}{R_{tot,F}} \tag{25}$$

Figure 2 gives an illustration of the described variables for the cases with the most extreme insulation levels, L_EL_G and H_EH_G, and heating profiles, CH and P2. Since the exterior equivalent temperatures of the four cases nearly coincide, only the time series for case L_EL_G_P2 is displayed.

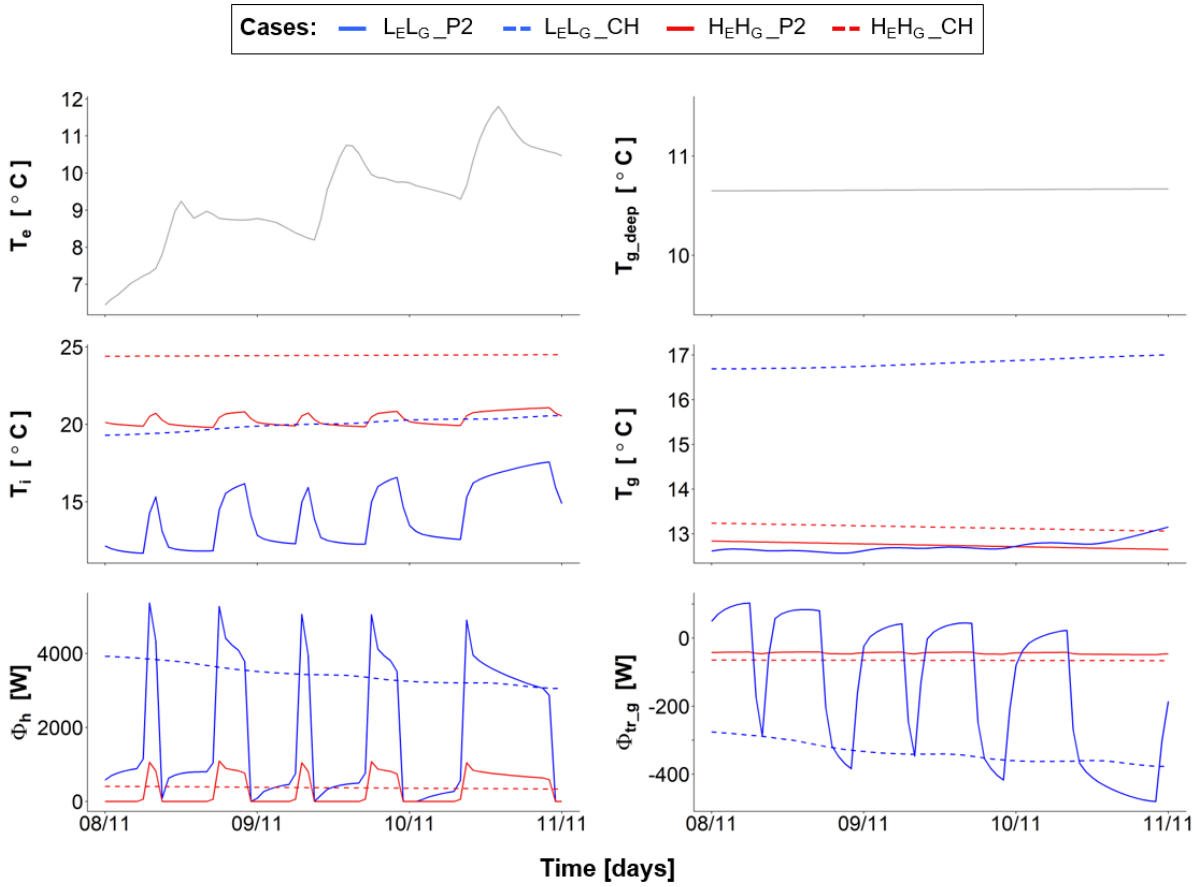

Figure 2: Time series plots of the output and input variables of the ARX-models for the four most extreme cases. Figures display hourly values.

Two times eight ARX-models are identified on the sixteen data sets using the 'linear model' ('lm') function [29]. The first group of models (set of Eqs. 'I') takes the net heat input Φ_h as output, the second one (set of Eqs. 'II') the interior temperature T_i. The variables that are taken into account depend on the considered scenario ('s1' to 's4'), as discussed in section 4. Additionally, for each scenario, two versions are proposed to evaluate the influence of a constant term: (1) adding an intercept term to the model structure, in which unmodeled, slowly varying physical phenomena can be lumped as suggested by [3] (see first Eq. of each scenario) or (2) forcing the model structure through the origin, to avoid wrongly attributing part of the constant phenomena to the intercept (second Eq. of each scenario).

$$
\mathrm{I}\begin{cases}
\mathrm{s1}\begin{cases}
\varphi(B)\cdot\Phi_{h;t} = \omega_i(B)\cdot T_{i;t} + \omega_e(B)\cdot T_{e;t} + \boldsymbol{\omega_g(B)}\cdot \boldsymbol{T_{g;t}} + \boldsymbol{int} + \varepsilon_t & (26)\\
\varphi(B)\cdot\Phi_{h;t} = \omega_i(B)\cdot T_{i;t} + \omega_e(B)\cdot T_{e;t} + \boldsymbol{\omega_g(B)}\cdot \boldsymbol{T_{g;t}} + \varepsilon_t & (9A)
\end{cases}\\
\mathrm{s2}\begin{cases}
\varphi(B)\cdot\Phi_{h;t} = \omega_i(B)\cdot T_{i;t} + \omega_e(B)\cdot T_{e;t} + \boldsymbol{int} + \varepsilon_t & (27)\\
\varphi(B)\cdot\Phi_{h;t} = \omega_i(B)\cdot T_{i;t} + \omega_e(B)\cdot T_{e;t} + \varepsilon_t & (12A)
\end{cases}\\
\mathrm{s3}\begin{cases}
\varphi(B)\cdot\left(\Phi_{h;t} - \Phi_{tr,g;t}\right) = \omega_i(B)\cdot T_{i;t} + \omega_e(B)\cdot T_{e;t} + \boldsymbol{int} + \varepsilon_t & (28)\\
\varphi(B)\cdot\left(\Phi_{h;t} - \Phi_{tr,g;t}\right) = \omega_i(B)\cdot T_{i;t} + \omega_e(B)\cdot T_{e;t} + \varepsilon_t & (17A)
\end{cases}\\
\mathrm{s4}\begin{cases}
\varphi(B)\cdot\Phi_{h;t} = \omega_i(B)\cdot T_{i;t} + \omega_e(B)\cdot T_{e;t} + \boldsymbol{\omega_g(B)}\cdot \boldsymbol{T_{g_{deep};t}} + \boldsymbol{int} + \varepsilon_t & (29)\\
\varphi(B)\cdot\Phi_{h;t} = \omega_i(B)\cdot T_{i;t} + \omega_e(B)\cdot T_{e;t} + \boldsymbol{\omega_g(B)}\cdot \boldsymbol{T_{g_{deep};t}} + \varepsilon_t & (30)
\end{cases}
\end{cases}
$$

$$
\text{II}\begin{cases}
\text{s1}\begin{cases}
\varphi(B)\cdot T_{i;t} = \omega_h(B)\cdot \Phi_{h;t} + \omega_e(B)\cdot T_{e;t} + \boldsymbol{\omega_g(B)}\cdot \boldsymbol{T_{g;t}} + \boldsymbol{int} + \varepsilon_t & (31)\\
\varphi(B)\cdot T_{i;t} = \omega_h(B)\cdot \Phi_{h;t} + \omega_e(B)\cdot T_{e;t} + \boldsymbol{\omega_g(B)}\cdot \boldsymbol{T_{g;t}} + \varepsilon_t & (9B)
\end{cases}\\
\text{s2}\begin{cases}
\varphi(B)\cdot T_{i;t} = \omega_h(B)\cdot \Phi_{h;t} + \omega_e(B)\cdot T_{e;t} + \boldsymbol{int} + \varepsilon_t & (32)\\
\varphi(B)\cdot T_{i;t} = \omega_h(B)\cdot \Phi_{h;t} + \omega_e(B)\cdot T_{e;t} + \varepsilon_t & (12B)
\end{cases}\\
\text{s3}\begin{cases}
\varphi(B)\cdot T_{i;t} = \omega_h(B)\cdot \left(\Phi_{h;t} - \Phi_{tr,g;t}\right) + \omega_e(B)\cdot T_{e;t} + \boldsymbol{int} + \varepsilon_t & (33)\\
\varphi(B)\cdot T_{i;t} = \omega_h(B)\cdot \left(\Phi_{h;t} - \Phi_{tr,g;t}\right) + \omega_e(B)\cdot T_{e;t} + \varepsilon_t & (17B)
\end{cases}\\
\text{s4}\begin{cases}
\varphi(B)\cdot T_{i;t} = \omega_h(B)\cdot \Phi_{h;t} + \omega_e(B)\cdot T_{e;t} + \boldsymbol{\omega_g(B)}\cdot \boldsymbol{T_{g_{deep};t}} + \boldsymbol{int} + \varepsilon_t & (34)\\
\varphi(B)\cdot T_{i;t} = \omega_h(B)\cdot \Phi_{h;t} + \omega_e(B)\cdot T_{e;t} + \boldsymbol{\omega_g(B)}\cdot \boldsymbol{T_{g_{deep};t}} + \varepsilon_t & (35)
\end{cases}
\end{cases}
$$

5.3.2. Model order selection

The training data sets consist of hourly values and span from November 1 to January 31, covering part of the heating season in Brussels.

All models are fitted according to the 'forward modelling' procedure outlined in [4]:

1. The order of the input polynomials is set equal to zero; no lags[5] are included. The order of the output polynomial is taken one higher than that of the input polynomials.
2. The model is fitted and subsequently examined for white noise residuals using the Autocorrelation Function (ACF) and Cumulated Periodogram (CP) [5]. The significance of the model coefficients is furthermore verified via a marginal t-test using a threshold of 0.05.
3. The model order is steadily increased until both of the following conditions are met:
    - The ACF and CP do not exceed the 95% two-sided statistical significance limits in more than 5 % of the time (visual verification).
    - The highest lag of the output polynomial and at least one lag of each input polynomial are significant. The significance of the intercept term is not taken into account.

Additionally, two new rules were adopted to avoid convergence problems when including near-zero variance predictors (see time series plots Figure 2) in the models:

- The order of the input polynomial ω_g is set equal to one, regardless of the order of the other polynomials. If no valid model can be obtained with the first lag of T_g (scenario 1) or T_{g_deep} (scenario 4) included, it is tried to obtain a valid model with only the value at time t=0 included.
- The almost constant signals for variables T_i and Φ_h in the models H_EL_G_CH and H_EH_G_CH cause some of the coefficients included in $\omega_h(1)$ and $\omega_i(1)$ to be indefinable because of singularities: the fitting procedure results in 'Not Available' coefficients (NA's). Therefore, the model order selection process is further adapted: if one or more model coefficients of either T_i or ϕ_h are not identifiable following the standard model order selection procedure, only the current value of the variable (lag 0) will be included in the model structure.

5.3.3. Model validation

The ACF and CP plots are inspected as part of the model selection procedure. The identified models are furthermore statistically validated by two cross validation tests.

In the first test, the model which was identified on the training period is used to predict the interior temperature (or net heat input in the case of models with Φ_h as output) for both 20 consecutive days of data embedded in the training data set and 20 consecutive days outside the training period, a so-called 'cross-validation period', using a 'one-step-ahead' approach. The 20-day periods were arbitrarily selected at the beginning of January and February for the training and cross validation period respectively. The 'one-step-ahead' approach assumes that all observations of both T_i and the input variables up to time t can be utilized to predict the value for T_i at time t+1.

Next, the normalized root mean square error nRMSE [%] between the simulated interior temperature (T_i) and the one-step-ahead predictions of the identified ARX model ($\hat{T}_i$) is determined as expressed in Eq. 36, with n the number of samples, namely 480 (20 days times 24 samples).

[5] Lag *n* is the value of the variable at time (t-*n*).

The risk of overfitting of the ARX-model is assessed by verifying that the nRMSE of the training and validation period are of the same order of magnitude. This test is particularly necessary since the lack of measurement noise of the synthetic data results in relatively high model orders (order of 33 up to 87 for the output polynomial).

$$nRMSE = \sqrt{\frac{\sum\left(T_i(t)-\hat{T}_i(t)\right)^2}{(n-1)}} \cdot \frac{100}{\left(T_{i,max}-T_{i,min}\right)} \tag{36}$$

In the second test, the goodness-of-fit of the models is examined by simulating the output variable for a 2-week cross-validation period in February using 'multiple-steps-ahead prediction'. In this approach, the one-step-ahead predictions of the output variable are fed back into the data set and used as input in following prediction steps instead of the actual observations. Hence, the prediction error propagates further, making it harder to obtain low nRMSE values. Models that are better capable of predicting the buildings' dynamic behavior (expressed by lower nRMSE numbers) are therefore assumed to have a more accurate internal structure. This supports the confidence in the HLC deduced from the model coefficients. The maximum nRMSE value obtained by all models with the interior temperature as output presented below is 6.44 %, for the models with the net heating power as output, the maximum value amounts to 4.25 %.

5.3.4. Identification of the HLCs

The mean estimates of HLC, HLC_e, HLC_i and HLC_g are deduced using the formulas devised in section 4 (Eqs. 10, 13 18 and 19). The associated uncertainties, represented by the 95% confidence intervals, are calculated via a simulation approach in which 10000 random realizations are made of the fitted polynomials [30].

6. RESULTS ANALYSIS AND DISCUSSION

The section below consecutively discusses the HLC estimates obtained for the four scenarios.

6.1. Scenario 1: Ground temperature (T_g) is monitored

Four different ARX-models (Eqs. 26, 9A, 31 and 9B) were proposed to analyze the sixteen OBM data sets under scenario 1. Figure 3 presents, for each of these models[6], the HLC_e estimates identified by applying Eqs. 10A and 10B on the fitted model coefficients. As the sixteen cases share two different reference values (261 W/K and 17.3 W/K, see Table 3), the graph is split into two: the cases with insulation levels L_EL_G and L_EH_G, and H_EL_G and H_EH_G, are respectively plotted on the same vertical scale. This allows a visual assessment of the relative importance of the estimation errors. Similarly, Figures 4 and 5 give an overview of the characterization outcomes for respectively performance indicators HLC_g and the HLC_i.

The good agreement between the HLC_e, HLC_i and HLC_g estimates and their respective reference values provides a strong indication that the adopted rules regarding the physical meaning of the model coefficients (Eqs. 10) are valid.

The model with T_i as output and a zero-intercept provides the best results, by showing significantly lower errors and consistent results for all criteria. From the results in Figures 3 to 5, it appears that more precise HLC estimates are obtained by forcing the model structure through zero (compare the first with the second column for models with T_i as output, and the third with the fourth column for models with ϕ_h as output), although allowing a non-zero intercept not necessarily results in erroneous or highly uncertain estimates. When the setpoint temperature is held constant in well-insulated buildings (cases H_EL_G_CH and H_EH_G_CH) it nevertheless becomes impossible to obtain a statistically valid model with a non-zero intercept. After all, the ϕ_h signal itself is then nearly constant, as can be seen from Figure 2 for the H_EH_G-case. Additionally, the wall and roof insulation cause the interior

[6] Model equations are written without the coefficients to be fitted.

equivalent temperature represented by T_i to nearly equal the interior air temperature, which is thermostatically controlled at 25 °C.
Opting for a model parametrization with ϕ_h as output instead of T_i only leads to minor deviations (up to 2.3 %) on the mean estimate, in the case of the zero intercept. Meanwhile, the range of the 95% confidence interval (CI) is on average 168 % larger. Since it was more frequently impossible to identify a valid model with ϕ_h as output, preference is given to the parametrization with T_i as output.

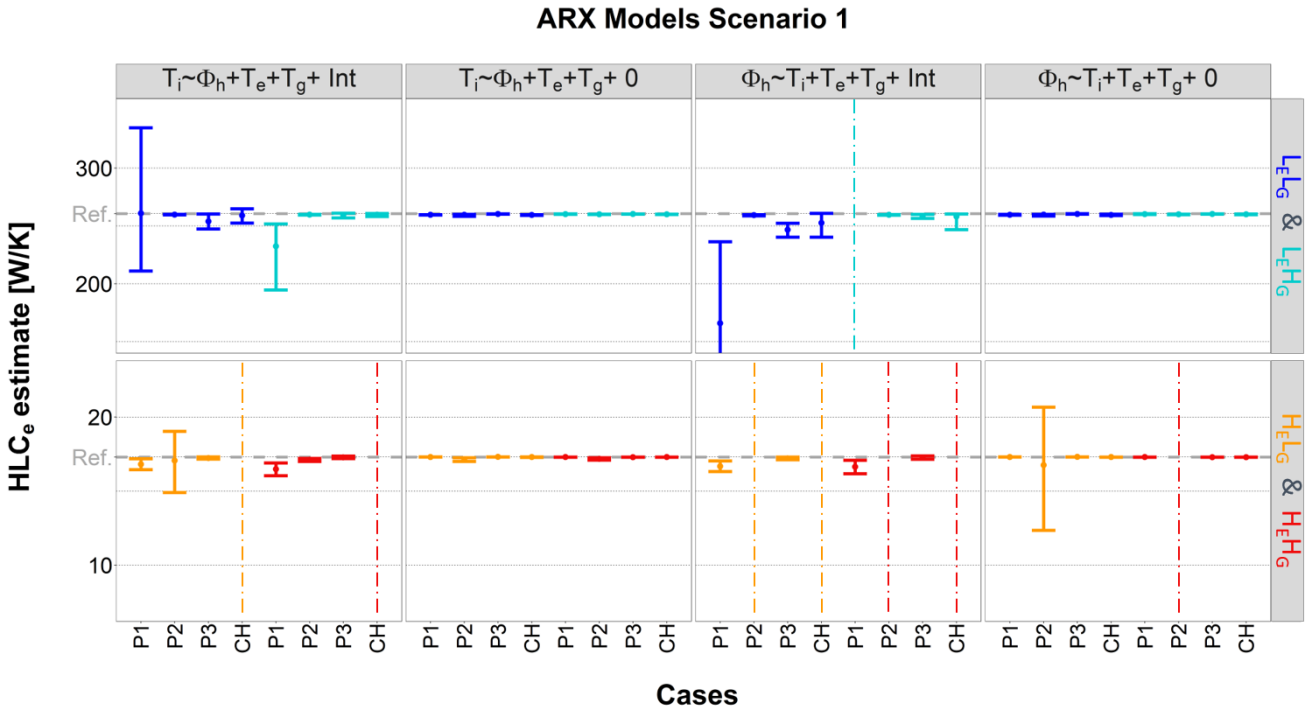

Figure 3: Identification of four different ARX-models on the sixteen case study data sets. The resulting HLC_e estimates are compared to the performance indicator's reference values ('Ref'). The dots indicate the mean estimates, the whiskers represent the 95% confidence intervals. The dot-dashed vertical lines mark invalid models.
The two models on the left use the interior temperature as output, the two on the right the net heat input. The models alternately include a non-zero and zero intercept. P1, P2 and P3 respectively represent the slightly, highly and moderately varying heating profile and CH the constant heating profile. L and H resp. stand for the low and high insulation level, subscripts E and G for the building elements in contact with the exterior environment and ground.

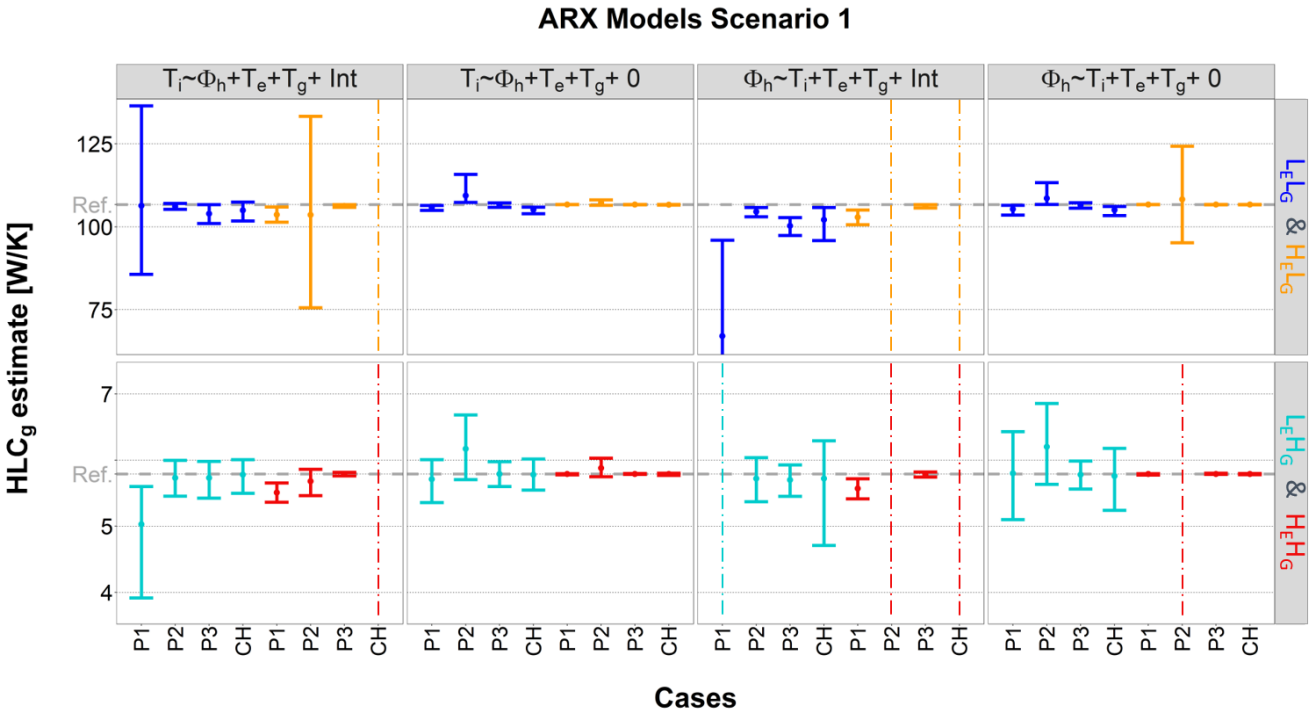

Figure 4: Identification of four different ARX-models on the sixteen case study data sets. The resulting HLC_g estimates are compared to the performance indicator's reference values ('Ref'). The dots indicate the mean estimates, the whiskers represent the 95% confidence intervals. The dot-dashed vertical lines mark invalid models.
The two models on the left use the interior temperature as output, the two on the right the net heat input. The models alternately include a non-zero and zero intercept. P1, P2 and P3 respectively represent the slightly, highly and moderately varying heating profile and CH the constant heating profile. L and H resp. stand for the low and high insulation level, subscripts E and G for the building elements in contact with the exterior environment and ground.

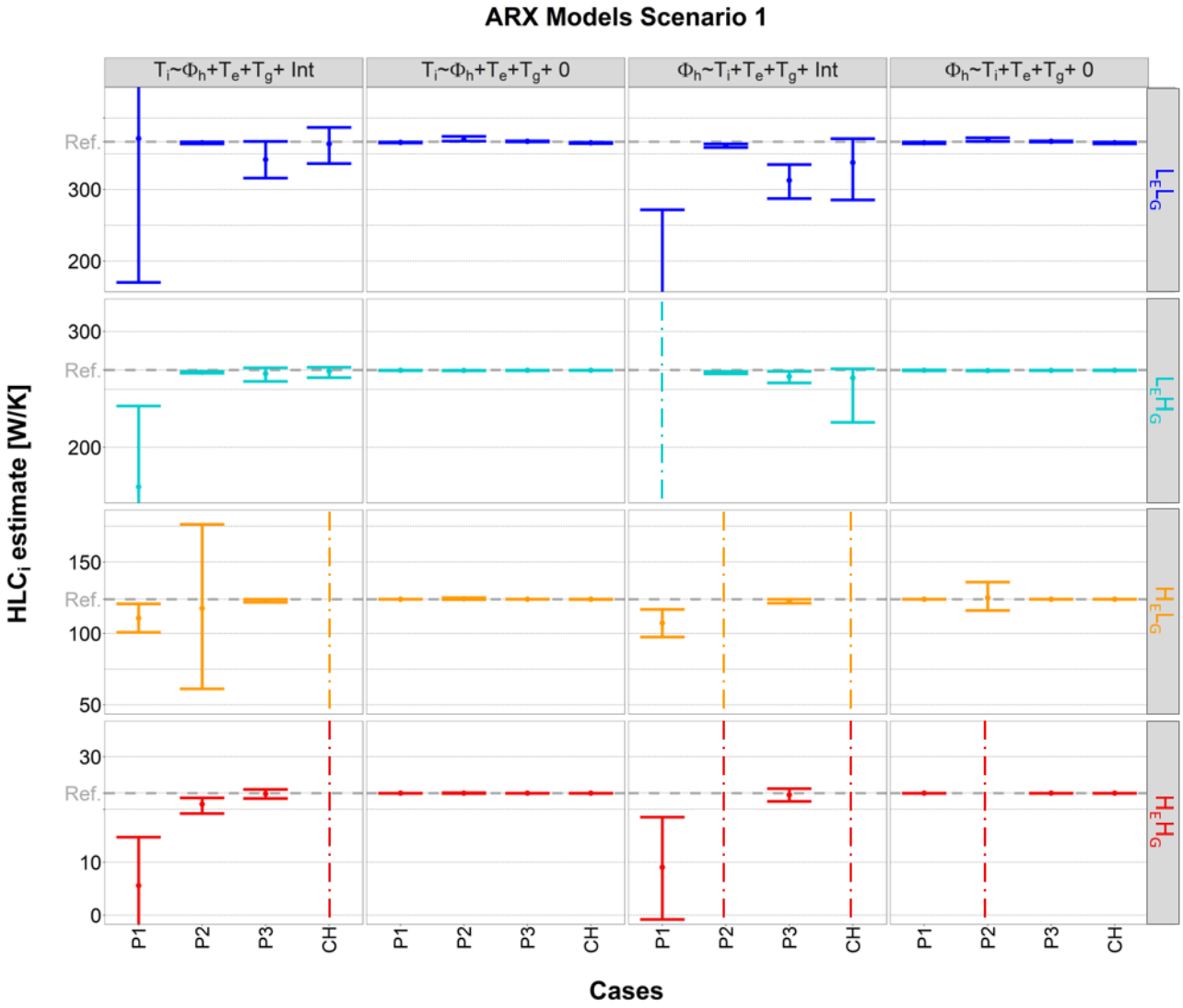

Figure 5: Identification of four different ARX-models on the sixteen case study data sets. The resulting HLC_i estimates are compared to the performance indicator's reference values ('Ref'). The dots indicate the mean estimates, the whiskers represent the 95% confidence intervals. The dot-dashed vertical lines mark invalid models.
The two models on the left use the interior temperature as output, the two on the right the net heat input. The models alternately include a non-zero and zero intercept. P1, P2 and P3 respectively represent the slightly, highly and moderately varying heating profile and CH the constant heating profile. L and H resp. stand for the low and high insulation level, subscripts E and G for the building elements in contact with the exterior environment and ground.

6.2. Scenario 2: No data on ground heat losses available

In practice, it is unlikely to obtain a reliable measurement of the ground temperature under the floor slab of an occupied building. Therefore, T_g is not included as an input in the ARX-models in this second scenario.
Figure 6 presents the HLC estimates obtained by applying Eqs. 32 and 12B on the 4 cases with the heating profile with moderately changing set point, P3, and analyzing the fitted model coefficients in accordance with Eq. 13B. The results of the cases with heating profiles P1, P2 and CH, and the outcomes of the ARX-models with Φ_h as output are similar, and hence not shown here.

Since the ground temperature is nearly constant at greater depth (see T_{g_deep} Figure 2), Eq. 32, with T_i as output, tries to represent this unmonitored variable by a constant intercept in the model structure. Figure 6 demonstrates that this approach leads to underestimations up to 50 % for cases P3 (up to 59 % for all heating profiles). Moreover, the reference values are not even included in the 95% CI, except for the uninsulated cases (L_EL_G). The underestimations indeed prove to be more pronounced for the more insulated dwellings: the underestimation of the reference value by the mean estimate is maximally 1.9 %, 7.9 %, 21 % and 59 % for respectively cases L_EH_G, L_EL_G, H_EH_G and H_EL_G.
The HLC estimates based on Eq. 12B with its zero-intercept, on the other hand, are rather accurate: for 13 out of the 16 cases the reference value is included in the estimated 95% CI and the maximal deviation between the mean estimate and the reference value is 2.25 % for cases P3 and 6.59 % for all heating profiles. However, the range of the 95% CI's are the quite large, amounting up to 35.1 % of the mean estimates.
The setback of the estimation accuracy compared to scenario 1 is also slightly noticeable in the nRMSE scores obtained for the prediction test on cross-validation data (see section 5.3.3). Where the average nRMSE value of the models with T_i and Φ_h as output amounts to respectively 0.42 % and 1.01 % under scenario 1, these values increase to respectively 0.95 % and 1.18 % under scenario 2.[7]

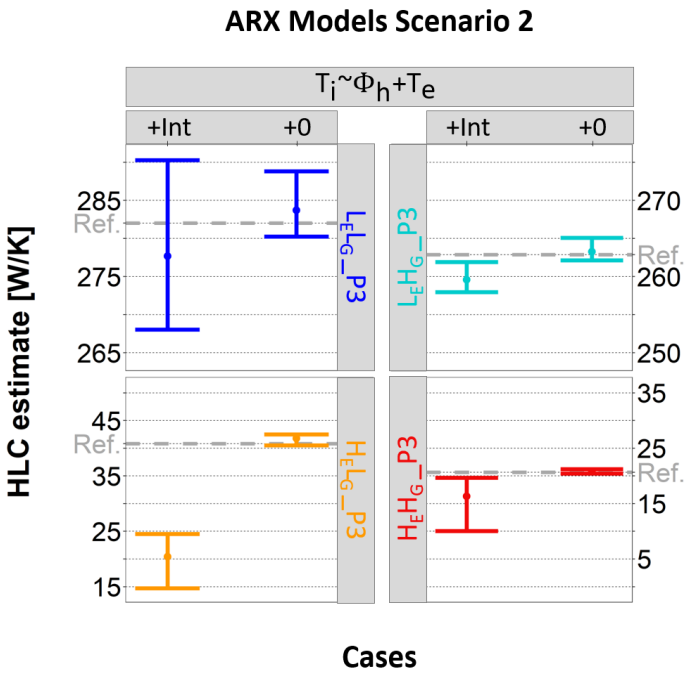

Figure 6: Identification of two different ARX-models (one with and one without intercept) on case studies with heating profile P3 under Scenario 2. The resulting HLC estimates are compared to the performance indicator's reference values ('Ref'). The dots indicate the mean estimates, the whiskers represent the 95% confidence intervals.
L and H resp. stand for the low and high insulation level, subscripts E and G for the building elements in contact with the exterior environment and ground.

In §4.2 the hypothesis was raised that the steady-state gains from which the HLC-estimates in Figure 6 are inferred, H_i and H_e, would also approximate the HLC (Eq. 13B). Figure 7 shows this theory cannot be justified for the cases in which heating profile P3 is applied[8].
For insulation levels L_EL_G and L_EH_G the values of H_i and H_e are still relatively close to one another and to

[7] Results obtained for the models with zero-intercept. All cases (heating profiles and insulation levels) are taken into account.
[8] Again, similar findings are obtained for the cases with other heating profiles (P1, P2, CH), and for the ARX models with ϕ_h as output. The results from the models with ϕ_h as output will therefore not be numerically discussed.

H, with H_e being maximally 1.25 % lower than H for cases P3 (maximally 7.78 % when considering all 4 heating profiles). The Lagrange weighting had, by contrast, a large impact on the uncertainty associated with H. Parameter H_e has the widest 95% CI's, with a range of up to 48.0 W/K for case L_EH_G_CH. The minimum variance weighting hence reduced the ranges of the 95% CI's of H_e considerably towards those of H: with up to 74.5 % for cases P3 and up to 90.2 % in general.
The higher insulation levels H_EL_G and H_EH_G on the other hand lead to more deviating estimates for H_e, H_i and H. For heating profile P3, H_e-values of up to 50.3 % lower than the H values can be observed (Figure 7). In the case of H_EL_G_P2, the H_e-estimate is even 6.78 times higher than the one for H. In the majority of the H_EL_G and H_EH_G-cases, but also in the case of L_EL_G_P2 and L_EH_G_P2, the 95% confidence intervals of the H_i and/or the H_e-estimates do not overlap with the reference value. The value of H_e even seems to tend more towards the reference value of HLC_e. This does not seem to be the case for H_i and HLC_i. For example, HLC_i equals 124 W/K for the H_EL_G-cases (see Table 3).

If the ground heat losses cannot be explicitly modelled in the ARX parametrization, it is recommended to set the intercept term equal to zero and to apply Langrage weighting on the identified H_i and H_e-parameter.

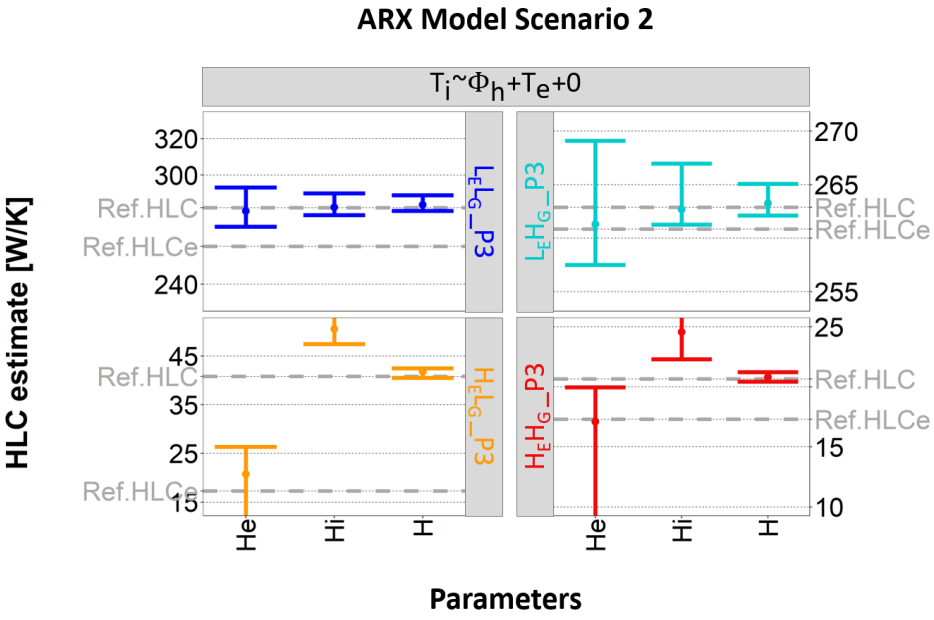

Figure 7: Comparison of the H_e, H_i and H-parameter obtained by identifying an ARX model with T_i as output and zero-intercept on the data sets of the cases with heating profile P3. The dots indicate the mean estimates, the whiskers represent the 95% confidence intervals.
L and H resp. stand for the low and high insulation level, subscripts E and G for the building elements in contact with the exterior environment and ground.

6.3. Scenario 3: Transmission heat losses to the ground ($\phi_{tr,g}$) are monitored

The third scenario uses the ARX-models with zero-intercept in Eqs. 17 to investigate whether the availability of heat flux meter data measuring the heat flux through the slab-on-ground allows to determine the HLC_e. Not only in the case of the heating profile with the moderately changing set point P3 (shown in Figure 8), but also for the other synthetic data sets, the Lagrange weighted average H (Eqs. 18) indeed closely approximates the sum of the U*A-values of the building elements in contact with the external environment. Only in the cases H_EL_G and H_EH_G some model validation issues occur when (ϕ_h+$\phi_{tr,g}$) is taken as model output (Eq. 17A). In contrast with scenario 2, H_i and H_e closely align with H and the reference value, and their 95% CI's are small.
The models under this third scenario obtain the best results for the cross validation test (section 5.3.3), with an average nRMSE score of 0.41 % for the models with T_i as output and zero-intercept and 0.89

% for the models with ϕ_h as output and zero-intercept (considering all cases).
Although the uncertainty on the estimates is small, and the mean estimates deviate only minimally from the reference value (up to 0.21 % for cases P3, 0.44 % for all heating profiles)[9], it should be noted that the reference value is not always included in the 95% CI. The 97.5 percentile (upper whisker in the plots) underestimates the reference value with up to 0.14 % for the cases P3 (0.37 % for all heating profiles). Since this error is quite limited, it is considered to be acceptable for most applications. Hence, adding heat flux sensors on the slab-on-ground yields better estimates for the heat transfer through the walls and roof.

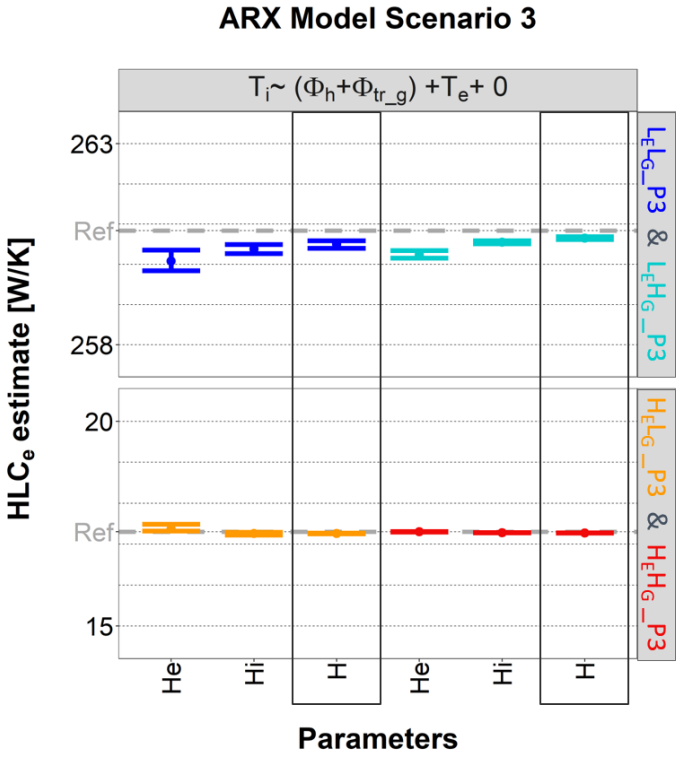

Figure 8: Identification of an ARX model with T_i as output on six case studies with heating profile P3 in order to assess the performance indicator HLC_e. The estimate 'H' is verified against the reference value ('Ref') and compared with the two parameters it is deduced from: H_e and H_i. The dots indicate the mean estimates, the whiskers represent the 95% confidence intervals.
L and H resp. stand for the low and high insulation level, subscripts E and G for the building elements in contact with the exterior environment and ground.

6.4. Scenario 4: Data analysis using a synthetic deep ground temperature (T_{g_deep})

Figure 9 shows how a synthetic deep ground temperature profile T_{g_deep} can be applied as a potential alternative for real measurement data to assess the HLC_e, at least when the slab-on-ground is insulated (cases L_EH_G and H_EH_G). Forcing the intercept equal to zero again seems a slightly better option. For cases with the uninsulated slab-on-ground floor, L_EL_G and H_EL_G, however, using T_{g_deep} in combination with a zero-intercept leads to underestimations of 3.8 % to 12 % and 6.4 % to 33 % respectively (mean estimate compared to reference value)[10]. As can be seen from Table 4, this deviation may be attributed to a larger discrepancy between the correlation of T_i and T_g and T_i and T_{g_deep}. Allowing a non-zero intercept here results in larger CI's. However, they do include the reference value. In 6 out of the 8 cases the mean estimate is also more accurate. The intercept term hence seems to compensate for the discrepancy between the synthetic T_{g_deep} and actual T_g.

[9] Given the similarity between the results of the ARX models with T_i and (ϕ_h+$\phi_{tr,g}$) as output, the numerical results presented in this section only consider the models with T_i as output.
[10] Numerical results for models with T_i as output.

In this scenario, adding a non-zero intercept to the model structure can be considered as a general solution to account for the unknown heat losses to the ground.

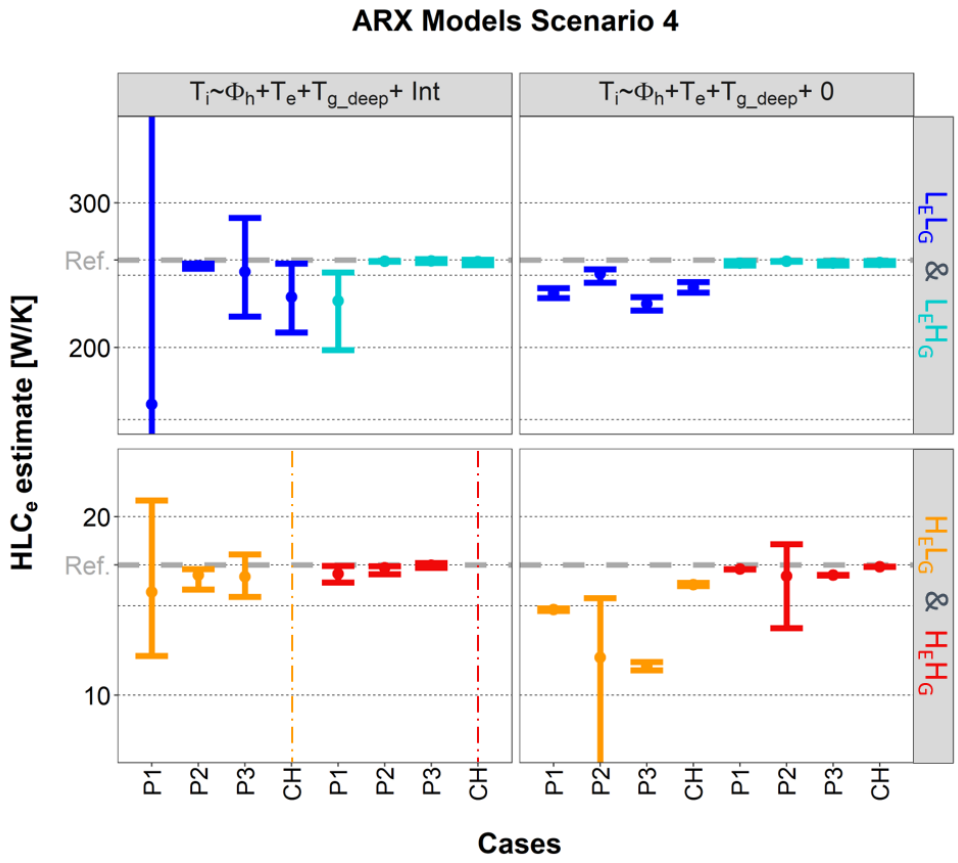

Figure 9: Identification of two ARX-models (one with and one without intercept) on the sixteen case study data sets. The resulting HLC_e estimates are compared with the performance indicator's reference values ('Ref'). The dots indicate the mean estimates, the whiskers represent the 95% confidence intervals. The dot-dashed vertical lines mark invalid models.
P1, P2 and P3 respectively represent the slightly, highly and moderately varying heating profile and CH the constant heating profile. L and H resp. stand for the low and high insulation level, subscripts E and G for the building elements in contact with the exterior environment and ground.

Table 4: Correlation coefficient between the interior equivalent temperature T_i and (1) the ground temperature T_g and (2) the undisturbed ground temperature at greater depth T_{g_deep}. The displayed values represent averages over the different heating profiles.

	Uninsulated floor slab		Insulated floor slab	
Cases	L_EL_G	H_EL_G	L_EH_G	H_EH_G
Correlation (T_i, T_g)	0.48	0.61	0.29	0.43
Correlation (T_i, T_{g_deep})	0.11	0.26	0.10	0.18
Difference between the correlation coefficients	0.37	0.36	0.20	0.25

For the other two performance indicators, HLC_g and HLC_i, no reliable estimates are obtained. The mean estimates for HLC_g exhibit deviations of 42.7 % to 306 % from their reference values[11]. These

[11] models with T_i as output, both with and without intercept (Eqs. 34-35)

latter are moreover only in a few cases included in the predicted 95% CIs. The estimates for H_EL_G are again the most erroneous.
These errors regarding HLC_g may have propagated to the HLC_i estimates, since from Figure 10 it can be seen that the characterization results of cases H_EH_G do not correspond to their reference values, in contrast to the correspondence for HLC_e. The underestimations of cases L_EL_G and H_EL_G are also more important.
Strikingly, the inaccuracy of the characterization outcome under this scenario is not reflected in the score that the models achieve for the cross validation test. The nRMSE value obtained by the models with T_i as output and non-zero intercept equals on average 0.48 %. For the models with ϕ_h as output and non-zero intercept this value amounts to 1.16 %. Hence, based on these results, the assumption that the predictive capability of the ARX models can be used as a measure for the accuracy of their HLC estimates, can be questioned.

The fact that (1) the estimation of HLC_e requires an intercept term in the model structure, which was discommended in the previous scenarios, and that (2) HLC_i and HLC_g cannot be reliably estimated, builds less trust in use of T_{g_deep} to model the heat losses to the ground.

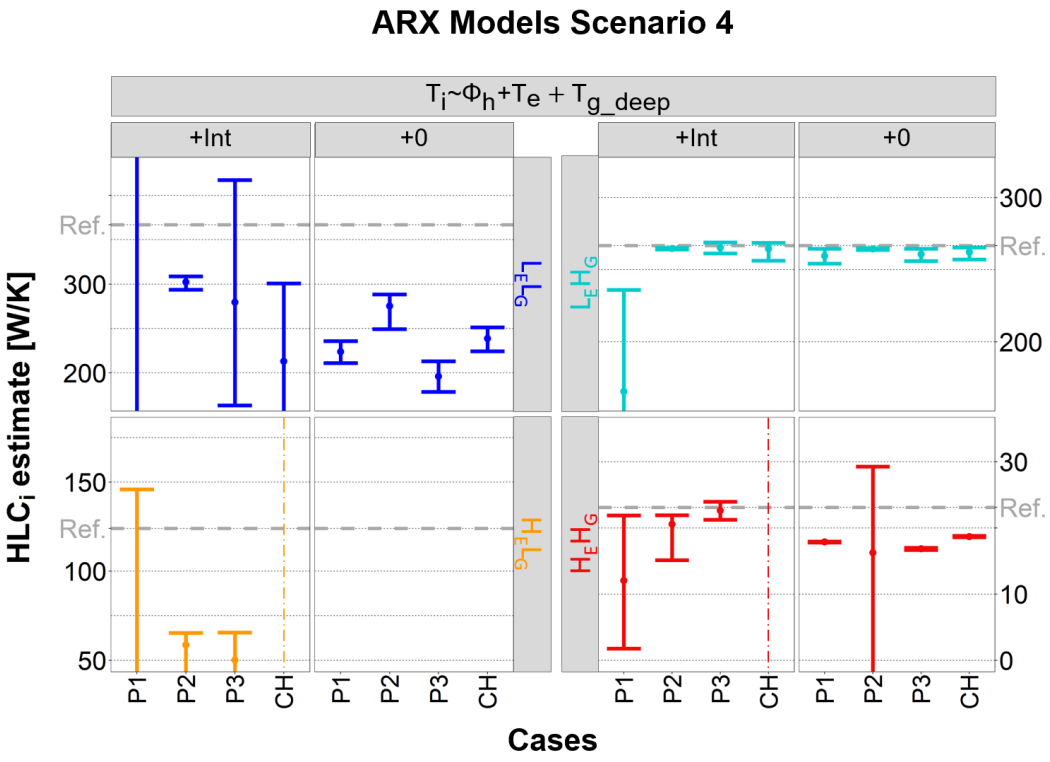

Figure 10: Identification of two ARX-models (one with and one without intercept) on the sixteen case study data sets. The resulting HLC_i estimates are compared with the performance indicator's reference values ('Ref'). The dots indicate the mean estimates, the whiskers represent the 95% confidence intervals. The dot-dashed vertical lines mark invalid models.
The 97.5th percentile (upper whisker) of the estimates of the model with zero-intercept for cases H_EL_G ranges between -66.9 W/K and 10.8 W/K.
P1, P2 and P3 respectively represent the slightly, highly and moderately varying heating profile and CH the constant heating profile. L and H resp. stand for the low and high insulation level, subscripts E and G for the building elements in contact with the exterior environment and ground.

6.5. Overall comparison

Finally, Table 5 compares all the estimates that were obtained by applying the models with T_i as output and a zero-intercept in case of scenario 1 to 3 and a non-zero intercept in case of scenario 4. The rows represent the 4 scenarios (abbreviated as 's1' to 's4') and the 4 key performance indicators, listed in Table 1, are arranged as column headings. The gray shades show that it is possible to assess HLC_i, HLC_e and HLC_g when an input for the ground temperature (be it a real (T_g, s1) or synthetic (T_{g_deep}, s4) one) is available. Otherwise (s2), only the HLC with its embedded temperature factor can be assessed. Using the heat flux to the ground as alternative input for the ground heat losses (s3) the HLC_e can be estimated as discussed in section 6.3. These heat flux measurements could additionally be used to assess the thermal transmittance of the slab-on-ground floor, and thus indirectly also the HLC_g and HLC_i.

For each scenario, the reliability of the characterization outcomes is evaluated using two criteria: (1) whether or not the reference value is included in the estimated 95% confidence interval (CI) [12] and (2) whether or not the maximal deviation of the outcome from the reference value is limited to 2 % or 10 %. The 'maximal deviation' is hereby taken as the maximal difference between either the 2.5th or the 97.5th percentile of the outcome (resp. $HLC_{2.5}$ and $HLC_{97.5}$) and the reference value (HLC_{ref}), divided by the reference value (Eq. 37). The 16 cases considered in each scenario are taken together in the evaluation: the first criterion is expressed as the percentage of the 16 cases for which the reference value is included in the 95% CI[13] and for the second criterion the case with highest deviation is decisive. Hence, the figures present the worst case result when no prior information is available on the building envelope assembly or heating profile.

$$\text{Max dev} = max\left(\left|\left(HLC_{2.5} - HLC_{ref}\right)\right|, \left|\left(HLC_{97.5} - HLC_{ref}\right)\right|\right) / HLC_{ref} \quad (37)$$

As can be seen from the table, even for the first scenario, where all input temperatures are measured, the reference value does not always lie within the range of the 95% CI of the estimates. This especially holds for HLC_e, where less than half of the cases (37.50 %) is 'accurate' in the meaning of 'including the actual performance indicator'. However, since their 95% CI's are small (they do not even exceed the 2% limit), the estimates are very precise. As an example for this behavior one could look at the estimate obtained for HLC_e in case L_EH_G_P2 (see also Figure 3). The range of the estimate is between 259.80 W/K and 260.17 W/K. The reference value is 260.85 W/K, meaning that the reference is not included in the 95% CI even if the maximal deviation is only 0.40 %.

Characterizing the energy performance without data on the ground heat losses (scenario 2) results in HLC estimates that are less precise (maximal deviation ranging between 0.50 % and 27.47 %), but their larger 95% CI's do include the reference value in 81.3 % of the cases. The maximal deviation from the reference value can be reduced by installing heat flux sensors on the slab-on-ground (scenario 3). This does change the reference from the HLC to the less comprehensive HLC_e. Chances are in this case high that the exact reference value is not included in the 95% CI. Given the small maximal deviation (0.55 %), the error is nonetheless small.

Explicitly including the ground heat losses via the input T_{g_deep} gives no assurance that the actual performance indicator is included in the 95 % or that the deviation from the reference value is limited to 10 %. Regarding the HLC_e estimates the max deviations prove to be higher for the buildings with uninsulated floor (62.70 %) than for those with insulated floor slab (24.00 %).

[12] In this calculation both the reference value and the percentiles are rounded to the nearest hundredth.

[13] The invalid models are counted as 'reference value not included in 95% CI'.

Table 5: Overview of the performance indicators that can be assessed in each of the scenarios (gray shades) and evaluation of the reliability of the estimates based on two criteria: (1) percentage of the cases in which the reference value lies within the range of the 95% CI of the estimate; and (2) maximal deviation of the estimate from the reference value.

	HLC			**HLC_i**			**HLC_e**			**HLC_g**		
	In 95% CI?	**Max dev**		**In 95% CI?**	**Max dev**		**In 95% CI?**	**Max dev**		**In 95% CI?**	**Max dev**	
		< 2%	**< 10%**		**< 2%**	**< 10%**		**< 2%**	**< 10%**		**< 2%**	**< 10%**
s1	/	/	/	62.5 %	yes	yes	37.5 %	yes	yes	93.8 %	no	no
s2	81.3 %	no	no	/	/	/	/	/	/	/	/	/
s3	/	/	/	/	/	/	12.5 %	yes	yes	/	/	/
s4	/	/	/	37.5 %	no	no	37.5 %	no	no	0.00 %	no	no

7. CONCLUSION

This paper uses sixteen synthetic data sets to examine under which circumstances and how the model coefficients of Auto-Regressive models with eXogenous inputs, identified on on-board monitoring data, can be related to the energy performance indicator 'Heat Loss Coefficient' ('HLC'). It demonstrates how the most precise characterization of the individual heat loss coefficients for the building elements in contact with the exterior environment ('HLC_e') and for the slab-on-ground ('HLC_g') can be made by identifying an ARX-model with the interior temperature as output and a zero-intercept on a monitoring data set including the ground temperature.

Since monitoring the ground temperature is often not possible in practice, an alternative could be to monitor the transmission heat losses to the ground. At that moment, HLC_e can be precisely estimated. In both situations, the maximum deviation of the HLC_e estimate from the calculated reference value is less than 2 %. The reference value itself might, however, not be included in the confidence interval. When no measurement data is available of the ground temperature or the ground transmission heat losses, a constant intercept term or a synthetic deep ground temperature could be used to model the ground heat losses. These approaches, however, prove less reliable, both in terms of inclusion of the reference value in the estimated 95% confidence interval, as with regard to the maximal deviation of the estimate from the reference.

By not explicitly modelling the ground heat losses still an overall HLC, which includes a temperature correction factor for the ground temperature, can be determined. The 95% confidence mainly (81.3% of the cases) includes the reference value, but might nevertheless be quite large (up to 35.1 % of the mean estimate)[14].

Further research should investigate whether and to what extent physical phenomena that were not yet taken into account (e.g. solar radiation, thermal inertia, internal heat gains, ventilation and infiltration air flow, etc.) affect these conclusions. By repeating the study on real measurement data, it could furthermore be verified how limitations of current measurement set-ups affect the characterization outcome.

ACKNOWLEDGEMENT

The authors gratefully acknowledge the Research Foundation Flanders (FWO) and the Flemish Institute for Technology (VITO) for funding this research (application number 1131918N).

REFERENCES

[1] R. Jack, Building Diagnostics: Practical Measurement of the Fabric Thermal Performance of Houses, PhD thesis Loughborough University, UK, 2015.

[14] Both figures hold for a set-up with interior temperature as output and zero-intercept.

[2] F. Alzetto, D. Farmer, R. Fitton, T. Hughes, W. Swan, Comparison of whole house heat loss test methods under controlled conditions in six distinct retrofit scenarios, Energy Build. 168 (2018) 35–41. doi:10.1016/J.ENBUILD.2018.03.024.
[3] G. Bauwens, In situ testing of a building's overall heat loss coefficient, PhD thesis KU Leuven, Belgium, 2015.
[4] H. Madsen, P. Bacher, G. Bauwens, A.H. Deconinck, G. Reynders, S. Roels, E. Himpe, G. Lethé, IEA EBC Annex 58: Report of Subtask 3, part 2: Thermal performance characterisation using time series data – statistical guidelines, KU Leuven, Leuven, 2016.
[5] H. Madsen, Time series analysis, Chapman & Hall/CRC, 2008.
[6] D. Johnston, D. Miles-Shenton, J. Wingfield, D. Farmer, M. Bell, Whole House Heat Loss Test Method (Coheating), 2012. http://www.leedsmet.ac.uk/as/cebe/projects/iea_annex58/whole_house_heat_loss_test_method(coheating).pdf.
[7] G. Bauwens, S. Roels, Co-heating test: A state-of-the-art, Energy Build. 82 (2014) 163–172. doi:10.1016/j.enbuild.2014.04.039.
[8] F. Alzetto, G. Pandraud, R. Fitton, I. Heusler, H. Sinnesbichler, QUB: A fast dynamic method for in-situ measurement of the whole building heat loss, Energy Build. 174 (2018) 124–133. doi:10.1016/j.enbuild.2018.06.002.
[9] P. Boisson, R. Bouchié, ISABELE method : In situ assessment of the building envelope performances, in: Proc. Ninth Int. Conf. Syst. Simul. Build., 2014: pp. 302–320.
[10] K.P. Subbarao, PSTAR - Primary and Secondary Terms Analysis and Renormalization. A Unifed Approach to Building Energy Simulation and Short-Term Monitoring, Sol. Energy Res. Inst. Golden, CO, USA. SERI/TR-25 (1988).
[11] European Commission, Clean energy for all - The new Energy efficiency measures, 2016. https://ec.europa.eu/energy/sites/ener/files/documents/technical_memo_energyefficiency.pdf.
[12] D. Saelens, G. Reynders, IEA EBC Annex 58: Report of Subtask 4b: Towards a characterisation of buildings based on in situ testing and smart meter readings and potential for applications in smart grids., Leuven, 2016.
[13] M. Senave, G. Reynders, S. Verbeke, D. Saelens, A simulation exercise to improve building energy performance characterization via on-board monitoring, Energy Procedia. 132 (2017) 969–974. doi:10.1016/j.egypro.2017.09.687.
[14] C. Ghiaus, F. Alzetto, Journal of Building Performance Simulation Design of experiments for Quick U-building method for building energy performance measurement Design of experiments for Quick U-building method for building energy performance measurement, (2019). doi:10.1080/19401493.2018.1561753.
[15] D. Farmer, D. Johnston, D. Miles-Shenton, Obtaining the heat loss coefficient of a dwelling using its heating system (integrated coheating), Energy Build. 117 (2016) 1–10. doi:10.1016/J.ENBUILD.2016.02.013.
[16] L. Ljung, System Identification: Theory for the User, 1999.
[17] P. Bacher, P.H.D. Andersen, IEA Common Exercise 4: ARX, ARMAX and grey-box models for thermal performance characterization of the test box, (2014) 49. http://orbit.dtu.dk/en/publications/iea-common-exercise-4-arx-armax-and-greybox-models-for-thermal-performance-characterization-of-the-test-box(029766fd-20dd-40ba-aa4e-6fe35e321337).html (accessed January 6, 2019).
[18] C. Ghiaus, Causality issue in the heat balance method for calculating the design heating and cooling load, (2013). doi:10.1016/j.energy.2012.10.024.
[19] M.J. Jiménez, H. Madsen, K.K. Andersen, Identification of the main thermal characteristics of building components using MATLAB, Build. Environ. 43 (2008) 170–180. doi:10.1016/J.BUILDENV.2006.10.030.
[20] S.A. Klein, W.A. Beckman, J.W. Mitchell, J.A. Duffie, N.A. Duffie, T.L. Freeman, J.P. Kummer, TRNSYS 17: A Transient System Simulation Program, (2009). http://sel.me.wisc.edu/trnsys.

[21] D.E. Bradley, M. Kummert, T.P. Mcdowell, Experiences with and Interpretations of Standard Test Methods of Building Energy Analysis Tools, in: Proc. IBPSA-Canada Bi-Annual Conf. ESIM 2004, 2004.
[22] D.B. Crawley, J.W. Hand, B.T. Griffith, Contrasting the capabilities of building energy performance simulation programs (version 1.0), 2005.
[23] P. Strachan, K. Svehla, I. Heusler, M. Kersken, Whole model empirical validation on a full-scale building, J. Build. Perform. Simul. (2015). doi:10.1080/19401493.2015.1064480.
[24] S.A. Klein, W.A. Beckman, J.W. Mitchell, J.A. et al. Duffie, TRNSYS 17: A Transient System Simulation Program: Multizone Building modeling with Type56 and TRNBuild, 5 (2012) 1–230.
[25] S.A. Klein, W.A. Beckman, J.W. Mitchell, J.A. et al. Duffie, TRNSYS 17: A Transient System Simulation Program: Mathematical Reference, 4 (2014) 474.
[26] ISO (International Organization for Standardization), ISO 13370: Thermal performance of buildings — Heat transfer via the ground — Calculation methods, 2017.
[27] J. Schietecat, Warmteoverdracht door wanden van gebouwen in contact met de grond. Toepassing van de rekenmethode uit de norm en ISO 13370. (in Dutch), 2002.
[28] ISO (International Organization for Standardization), ISO 6946: Building components and building elements — Thermal resistance and thermal transmittance — Calculation methods, 2017.
[29] R Core Team, R: A language and environment for statistical computing., (2017). https://www.r-project.org/.
[30] B. Efron, R. Tibshirani, Bootstrap Methods for Standard Errors, Confidence Intervals, and Other Measures of Statistical Accuracy, Stat. Sci. 1 (1986) 54–75. doi:10.2307/2245500.